Journal of Alloys and Compounds 509 (2011) 3096–3102

Contents lists available at ScienceDirect

Journal of Alloys and Compounds

journal homepage: www.elsevier.com/locate/jallcom

$LaPO_4:Eu^{3+}$, $LaPO_4:Ce^{3+}$, and $LaPO_4:Ce^{3+},Tb^{3+}$ nanocrystals: Oleic acid assisted solvothermal synthesis, characterization, and luminescent properties

Na Niu, Piaoping Yang*, Yan Wang, Wenxin Wang, Fei He, Shili Gai, Dong Wang

College of Material Science and Chemical Engineering, Harbin Engineering University, Harbin 150001, PR China

ARTICLE INFO

Article history:
Received 3 August 2010
Received in revised form 1 December 2010
Accepted 1 December 2010
Available online 9 December 2010

Keywords:
$LaPO_4$
Solvothermal synthesis
Luminescence
Oleic acid

ABSTRACT

$LaPO_4:Ln^{3+}$ (Ln = Eu, Ce, Tb) nanocrystals were successfully synthesized via a facile solvothermal process in the presence of oleic acid. The as-prepared crystals were well characterized by X-ray diffraction (XRD), transmission electron microscopy (TEM), X-ray photoelectron spectra (XPS), Fourier transform infrared spectroscopy (FT-IR), optical spectra as well as the kinetic decay times, respectively. In the synthesis process, oleic acid as a surfactant has played a crucial role in confining the growth and size of the $LaPO_4:Ln^{3+}$ phosphors. All the samples are well crystallized and assigned to the monoclinic monazite-type structure of the $LaPO_4$ phase. The prepared $LaPO_4:Ln^{3+}$ phosphors present a narrow distribution with an average particle size of about 15 nm. Upon excitation by ultraviolet radiation, the $LaPO_4:Eu^{3+}$ phosphors show the characteristic $^5D_0-^7F_{1-3}$ emission lines of Eu^{3+}, while the $LaPO_4:Ce^{3+},Tb^{3+}$ exhibits the characteristic $^5D_0-^7F_{3-6}$ emission lines of Tb^{3+}. It is believed that these rare earth ion doped (Eu^{3+} ion or Ce^{3+} and Tb^{3+} ions co-doped) monoclinic monazite-type $LaPO_4$ nanocrystals could find potential application as future advanced optical materials.

1. Introduction

Over the past decades, doping is a widely applied process in materials science which involves incorporating appropriate atoms or ions into host lattices to yield hybrid materials with desirable properties and functions [1–9]. Recently, a particular emphasis has been placed on the study of rare earth (RE) ions doped compounds due to their large variety of applications [10–18]. This is mainly based on their particular 4f–5d and 4f–4f electronic transition which can yield intense and narrow emission bands and thus generate individual colors in multi-phosphor devices [19–23]. However, the applications of RE-doped materials are still highly dependent on some basic factors such as size and morphology, which may govern their luminescence. Therefore, phosphors with special morphology, a fine particle size range, and non agglomeration can greatly improve the efficiency of luminescence, and brightness of the phosphors which are of significant value for their more broadly application [24]. Therefore, the synthesis of inorganic materials activated by RE ions with nano- or micro-sized and special morphology is a challenging issue which has attracted much research attention.

Rare earth orthophosphates ($LnPO_4$, Ln = La–Lu) have shown to be an excellent host lattice for lanthanide ions to prepare durable phosphors which can emit a variety of colors [25–27] and present many outstanding properties, including high insolubility [28], reliable stability against high temperatures and energy excitations [29], and high concentrations of lasing ions [30]. To date, lanthanum orthophosphates ($LaPO_4$) doped with different RE ions have been reported to be prepared through various methods, including solid-state reaction [31], microwave approach [32,33], sol–gel process [34–36], wet-chemical precipitation [37], hydrothermal method [38,39]. However, the practical applicability of these phosphates as phosphors is still limited by their light output, quantum yield and emission, which are directly influenced by their synthesis process to restrict their size, morphology, purity and stoichiometry. In consideration of this purpose, the solvothermal method is preferred because the synthesis conditions such as temperature and reaction time can be easily adjusted to gain the ideal morphology, phase and size of the products. Furthermore, the solvothermal process has proved to be a facile and fast route with low cost and energy consumption (reaction temperature <250 °C), which has been widely employed for the synthesis of other inorganic materials. Yet it has rarely been reported for the synthesis of rare earth ions doped $LaPO_4$ phosphors, especially for nano-sized lanthanum orthophosphates.

Herein, we presented a facile solvothermal process for the synthesis of RE ions doped $LaPO_4$ nanocrystals using oleic acid as capping agent in a mixed solvent. In this method, the organic capping ligand (oleic acid) has a profound effect on the growth of $LaPO_4$ phosphors via the adsorption of surfactants onto the surfaces of the nanocrystals. The structure, shape and luminescent properties of the obtained samples were well analyzed by means

* Corresponding author. Tel.: +86 451 8256 9890; fax: +86 451 8256 9890.
E-mail address: piaoping@ciac.jl.cn (P. Yang).

0925-8388/$ – see front matter © 2010 Elsevier B.V. All rights reserved.
doi:10.1016/j.jallcom.2010.12.008

Table 1
Calculated cell lattice constants and calculated average crystal sizes for $LaPO_4:Eu^{3+}$, $LaPO_4:Ce^{3+}$ and $LaPO_4:Ce^{3+},Tb^{3+}$.

Samples	*a*/deviation (Å)	*b*/deviation (Å)	*c*/deviation (Å)	*β* angle/deviation (Å)	*D*/crystal size (nm)
$LaPO_4$ (JCPDS 32–0493)	6.837	7.077	6.509	103.23	
$LaPO_4:Eu^{3+}$	6.833/0.004	7.067/0.01	6.502/0.007	103.37/0.14	15.7
$LaPO_4:Ce^{3+}$	6.834/0.003	7.071/0.006	6.499/0.01	103.43/0.2	16.2
$LaPO_4:Ce^{3+},Tb^{3+}$	6.813/0.024	7.043/0.034	6.479/0.03	103.55/0.33	15.3

of XRD, TEM, HRTEM, XPS, FT-IR, optical spectra and the kinetic decay times, respectively. A possible formation mechanism of the as-synthesized nanocrystals based on the capping effect of oleic acid was also proposed.

2. Experimental

2.1. Synthesis

All the chemical reagents including $(NH_4)_2HPO_4$ (A. R., Beijing Chemical Reagent Company), La_2O_3, Tb_4O_7, Eu_2O_3, $Ce(NO_3)_3{\cdot}6H_2O$ (99.99%, Science and Technology Parent Company of Changchun Institute of Applied Chemistry), oleic acid (A. R., Beijing Chemical Regent Company), NaOH (A. R., Beijing Chemical Regent Company), HNO_3 (A. R., Beijing Beihua Chemical Company) and ethanol (A. R., Beijing Beihua Chemical Company) were used without further purification.

The doping concentration of Eu^{3+} was 5 mol% to La^{3+} in $LaPO_4:Eu^{3+}$, which has been previously optimized [40]. Typically, 0.5 g of NaOH was added to the mixture of 4 mL oleic acid and 15 mL ethanol with continuous stirring to form an ivory white solution. Meanwhile, 0.95 mmol La_2O_3 and 0.05 mmol Eu_2O_3 were dissolved in dilute HNO_3 with vigorous stirring and heating. The superfluous HNO_3 was driven off until the $La(NO_3)_3$ and $Eu(NO_3)_3$ were obtained. Then the $La(NO_3)_3$ and $Eu(NO_3)_3$ powders were added into the pre-obtained solution with vigorous stirring until a translucent solution was obtained. After that, an aqueous solution containing 2 mmol of $(NH_4)_2HPO_4$ was poured into the above solution with strong magnetic stirring. After further stirred for another 2 h, the resulting solution was then transferred into a 50 mL sealed Teflon autoclave and statically heated at 180 °C for 12 h. When the autoclave was naturally cooled to the room temperature, the final product was separated by centrifugation, and washed several times with ethanol and distilled water. Finally, the obtained sample was dried in vacuum at 60 °C for 24 h. In this way, the $LaPO_4:Eu^{3+}$ nanoparticles were prepared.

The synthesis of the $LaPO_4:Ce^{3+}$ with the doping concentration of 20 mol% of Ce^{3+} to La^{3+} and the $LaPO_4:Ce^{3+},Tb^{3+}$ with the doping concentration of 20 mol% of Ce^{3+}, 15 mol% of Tb^{3+} to La^{3+} were similar to the above procedure.

2.2. Characterization

Powder X-ray (XRD) patterns were obtained on a Rigaku TR III diffractometer with Cu Kα radiation (λ = 0.15405 nm) with accelerating voltage and emission current of 40 kV and 200 mA. Transmission electron microscope (TEM) and high-resolution transmission electron microscope (HRTEM) were performed on a FEI Tecnai G^2 S-Twin transmission electron microscope with a field emission gun operating of 200 kV. The X-ray photoelectron spectra (XPS) were taken on a VG ESCALAB MK II electron energy spectrometer using Mg Kα (1253.6 eV) as the X-ray excitation source. Fourier transform infrared spectroscopy (FT-IR) was carried out in an ABB Bomen FTLA2000-100 spectrometer using KBr pellets. The UV–vis excitation and emission spectra were recorded on a Hitachi F-4500 spectrofluorimeter equipped with a 150 W xenon lamp as the excitation source. Luminescence decay curves were obtained from a Lecroy Wave Runner 6100 Digital Oscilloscope (1 GHz) using a 250 nm laser (pulse width = 4 ns, gate = 50 ns) as the excitation source (Continuum Sunlite OPO). All the measurements were carried out at room temperature.

3. Results and discussion

3.1. Phase purity and structure

The crystallinity and phase purity of the products were firstly examined by XRD analysis. Fig. 1 shows the typical X-ray diffraction (XRD) patterns of as-synthesized $LaPO_4:Eu^{3+}$, $LaPO_4:Ce^{3+}$, $LaPO_4:Ce^{3+},Tb^{3+}$ nanocrystals, and the standard data for monoclinic $LaPO_4$, respectively. As shown, the XRD patterns of all the $LaPO_4:Ln^{3+}$ nanocrystals are in good agreement with the values from JCPDS No. 32-0493 of $LaPO_4$, which reveals that all the products are monazite $LaPO_4$ with monoclinic structure in P21/n space group [41]. Furthermore, no additional peaks for other phases associated with the doped component can be observed, indicating a high purity of the RE ions doped $LaPO_4$ samples. Especially, there are three forms for lanthanide phosphates: hexagonal, tetragonal, and monoclinic. Considering that the commercial use of $LaPO_4$ phosphors are usually focus on monoclinic structure, the as-synthesized $LaPO_4$ nanophosphors can be directly used without further heat treatment. The calculated cell lattice constants and average crystal sizes for $LaPO_4:Ln^{3+}$ (Ln = Eu, Ce, Tb) samples are summarized in Table 1, together with the standard data (JCPDS No. 32-0493) for comparison. It can be seen that the calculated cell lattice constants (calculated from MDI Jade 5.0) for $LaPO_4:Eu^{3+}$, $LaPO_4:Ce^{3+}$, and $LaPO_4:Ce^{3+},Tb^{3+}$ are well consistent with the standard data (JCPDS No. 32-0493). In addition, it should be noted that the as-synthesized rare earth ions doped $LaPO_4$ samples show a slightly lower lattice constants compared with the standard data, which may be caused by the smaller ion radius of Eu^{3+}, Ce^{3+} and Tb^{3+} ions than La^{3+} ion (0.950 Å for Eu^{3+} ion, 1.034 Å for Ce^{3+} ion, 0.932 Å for Tb^{3+} ion, and 1.061 Å for La^{3+} ion). Moreover, it is clear that the diffractions of the XRD patterns show obvious broadening, suggesting the small size nature of the samples. The peak broadening can be used to estimate the average crystallite sizes by the Scherrer formula, $D = 0.89\lambda/\beta\cos\theta$, where D is the average grain size, λ is the X-ray wavelength (0.15405 nm), and θ and β are the diffraction angle and full-width at half-maximum (FWHM), respectively. The strongest three peaks (1 2 0) at $2\theta = 28.509°$, (0 1 2) at $2\theta = 30.898°$, and ($\bar{3}$ 1 1) at $2\theta = 41.882°$ were used to calculate the average crystallite size (D) of the sample. The average crystallite sizes for $LaPO_4:Eu^{3+}$, $LaPO_4:Ce^{3+}$, $LaPO_4:Ce^{3+},Tb^{3+}$ are estimated to be about 15.7 nm, 16.2 nm and 15.3 nm, respectively. This result is well consistent with the following TEM analysis.

3.2. Morphology, composition and the formation process

The morphologies of the $LaPO_4:Eu^{3+}$, $LaPO_4:Ce^{3+}$, and $LaPO_4:Ce^{3+},Tb^{3+}$ nanocrystals were carefully examined by TEM (Fig. 2). It can be seen that the three samples all have much similar shapes which are well-dispersed. The average particle size is about 10–20 nm which is in good agreement with the values calculated from the XRD patterns. Furthermore, there are no obvious

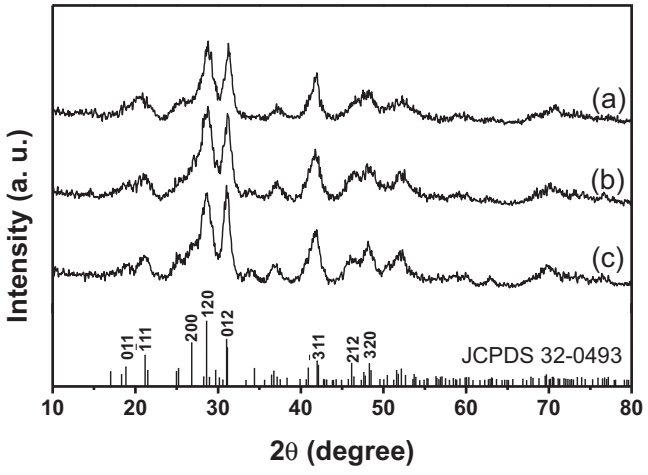

Fig. 1. X-ray diffraction patterns of as-synthesized $LaPO_4:Eu^{3+}$ (a), $LaPO_4:Ce^{3+}$ (b), $LaPO_4:Ce^{3+},Tb^{3+}$ (c), and the standard data for $LaPO_4$ (JCPDS No. 32-0493).

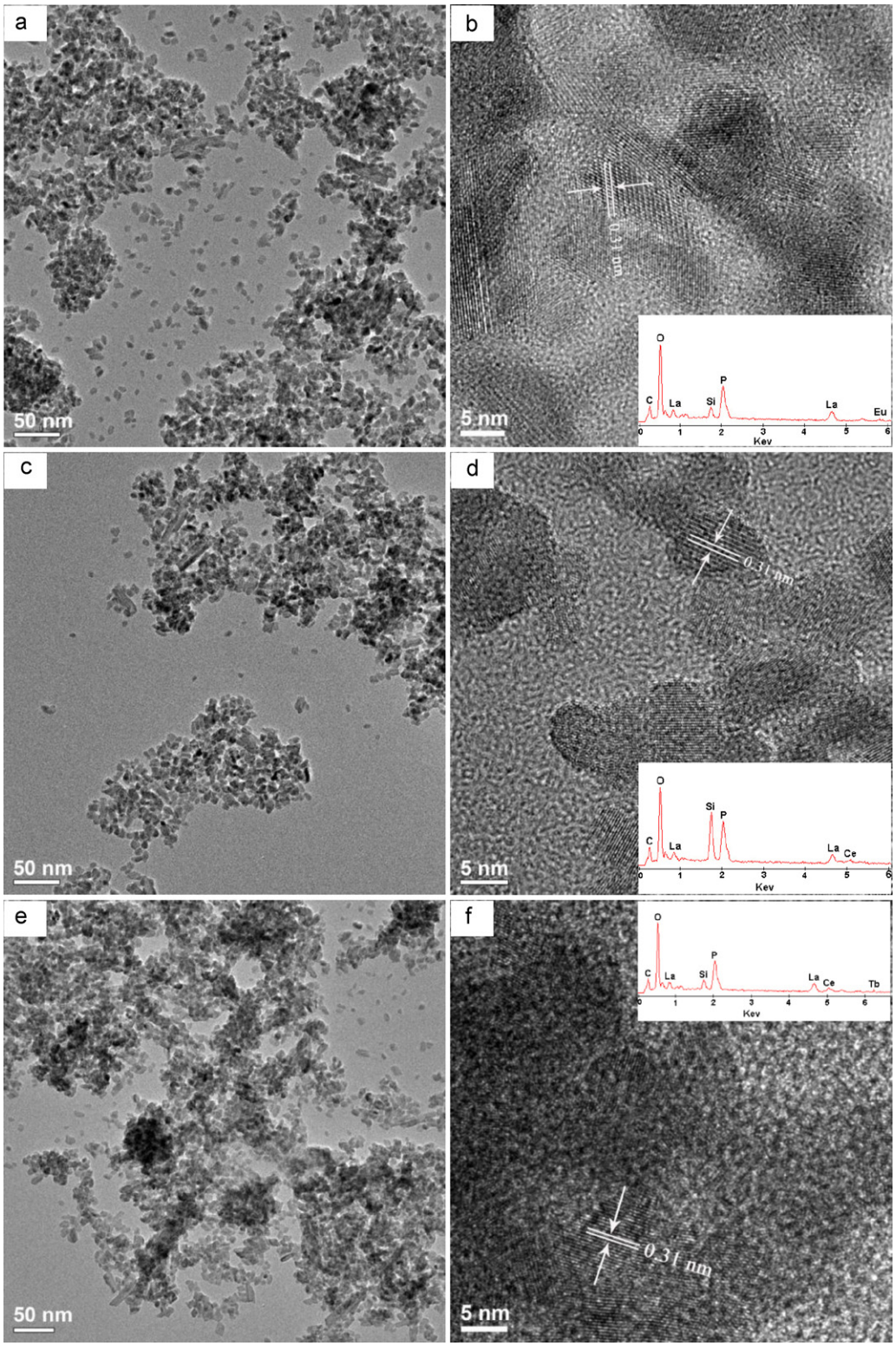

Fig. 2. Low-resolution TEM image (a), HRTEM image (b) of as-synthesized $LaPO_4:Eu^{3+}$; low-resolution TEM image (c), HRTEM image (d) of as-synthesized $LaPO_4:Ce^{3+}$; low-resolution TEM image (e), HRTEM image (f) of as-synthesized $LaPO_4:Ce^{3+},Tb^{3+}$; insets are their corresponding EDS.

discrepancy in particle size and morphology among the three samples, which means the doping components have little effect on the morphological features. The high-resolution TEM images of as-synthesized $LaPO_4:Eu^{3+}$, $LaPO_4:Ce^{3+}$, and $LaPO_4:Ce^{3+},Tb^{3+}$ samples are shown in Fig. 2b, d, and e, respectively. All the three images exhibit obvious lattice fringes which confirm the high crystallinity of the samples. The lattice fringes of (1 2 0) planes with an interplanar distance of 0.31 nm are marked by the arrow. The calculated interplanar distances between the adjacent lattice fringes agree well with the d_{112} spacing of the standard value (JCPDS No. 32-0493). Insets in Fig. 2b, d and e are the corresponding EDS analysis. In the EDS of $LaPO_4:Eu^{3+}$, the signals of lanthanum (La), phos-

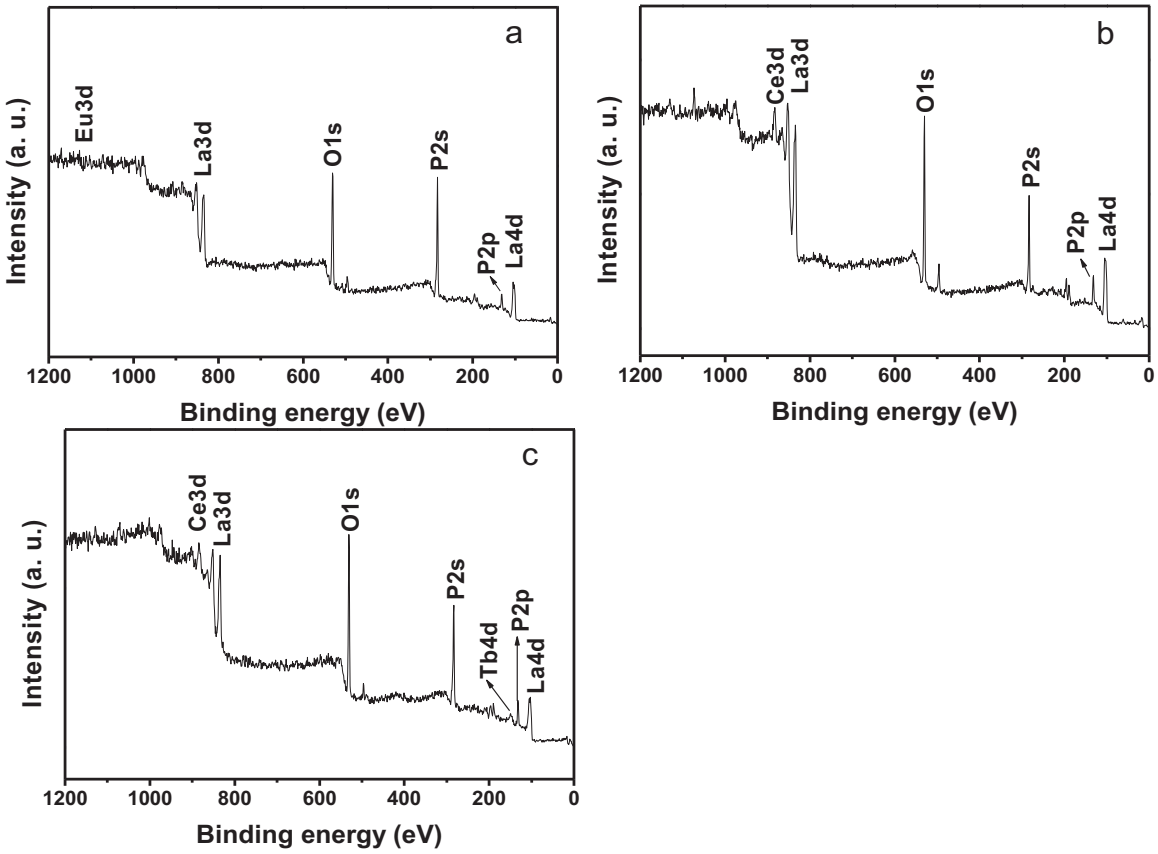

Fig. 3. The survey XPS of as-synthesized $LaPO_4$:Eu^{3+} (a), $LaPO_4$:Ce^{3+} (b), and $LaPO_4$:Ce^{3+},Tb^{3+} (c).

phorous (P), oxygen (O), europium (Eu) suggest the presence of corresponding element in the product (the carbon signal is due to the carbon used). Similarly, the signals of lanthanum (La), phosphorous (P), oxygen (O), cerium (Ce), and terbium (Tb) can also be seen in the EDS of $LaPO_4$:Ce^{3+} and $LaPO_4$:Ce^{3+},Tb^{3+} samples.

XPS of as-synthesized $LaPO_4$:Eu^{3+}, $LaPO_4$:Ce^{3+}, and $LaPO_4$:Ce^{3+},Tb^{3+} are shown in Fig. 3, respectively. The binding energy data (calibrated using C 1s (284.8 eV) as the reference) in the XPS of $LaPO_4$:Eu^{3+}, $LaPO_4$:Ce^{3+}, and $LaPO_4$:Ce^{3+},Tb^{3+} are well consistent with those reported for bulk $LaPO_4$ [42,43]. The peaks at about 1131 eV for Eu^{3+} (Fig. 3a), 885 eV for Ce^{3+} (Fig. 3b and c) indicate the binding energies of the $3d_{5/2}$ orbital of Eu^{3+} and Ce^{3+} in the corresponding $LaPO_4$:Ln^{3+} products. In addition, the binding energy of Tb (4d, 151 eV) for $LaPO_4$: Ce^{3+}, Tb^{3+} is also obvious. The peak at 133 eV (P 2p) for all the $LaPO_4$:Ln^{3+} phosphors indicate that the phosphorus in the products exists in a pentavalent oxidation state (P^{5+}) in the form of PO_4^{3-} [44]. And that the peaks at 531 eV (O 1s) and 838 eV (La 3d) for all $LaPO_4$:Ln^{3+} are also obvious. Furthermore, the calculated Eu/La/P molar ratio in $LaPO_4$:Eu^{3+} is 4.9/95.1/1, the calculated Ce/La/P molar ratio in $LaPO_4$:Ce^{3+},Tb^{3+} is 19.3/80.7/1, and the calculated Ce/Tb/La/P molar ratio in $LaPO_4$:Ce^{3+} is 20.3/14.9/64.8/1, which are very close to the stoichiometric values ($Eu_{0.05}La_{0.95}PO_4$, $Ce_{0.2}La_{0.8}PO_4$, $Ce_{0.2}Tb_{0.15}La_{0.65}PO_4$).

Fig. 4 gives the FT-IR spectra between 1500 cm^{-1} and 500 cm^{-1} of as-synthesized $LaPO_4$:Eu^{3+}, $LaPO_4$:Ce^{3+}, and $LaPO_4$:Ce^{3+},Tb^{3+}, respectively. As shown, the typical bands assigned to the phosphate groups (PO_4^{3-}) can be detected in the spectra. The band centered at 1019 cm^{-1} is a characteristic of the ν_3 anti-symmetric stretching of P–O band while the two bands located at between 621 and 538 cm^{-1} can be attributed to the ν_4 region of the vibrations of PO_4^{3-} groups. The shoulder at 952 cm^{-1} can be assigned to the ν_1

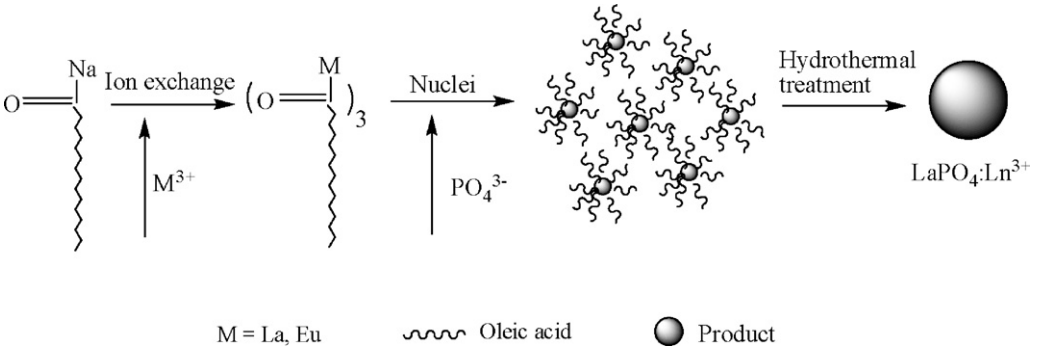

Scheme 1. Formation process of $LaPO_4$:Eu^{3+} nanocrystals.

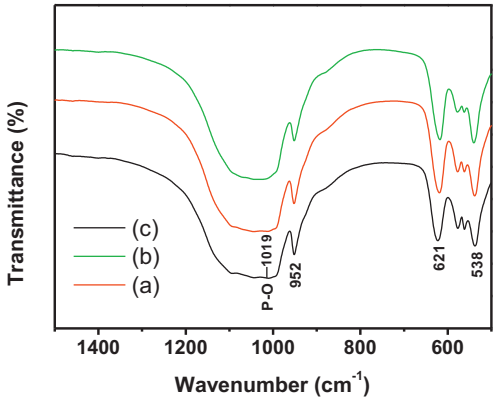

Fig. 4. FT-IR spectra of as-synthesized $LaPO_4:Eu^{3+}$ (a), $LaPO_4:Ce^{3+}$ (b), and $LaPO_4:Ce^{3+},Tb^{3+}$ (c).

vibration of PO_4^{3-} groups [45,46]. These bands are obvious characteristic of the vibrations of the phosphate groups in monoclinic $LaPO_4$.

The general formation process of the $LaPO_4:Ln^{3+}$ (Ln = Eu, Ce, Tb) nanocrystals could be understood by the combined aqueous and organic solvent-based synthetic route, which is similar to the previous reports [47–50]. In an organic solvent-based route, the starting materials are metal-organic complexes, while a water/ethanol mixed solution could be chosen as the main continuous inorganic solution phase. Since water is an ideal solvent for most inorganic salts and ethanol is a good solvent for most organic surfactants, most soluble inorganic salts can be employed as the starting materials, and long chain alkyl surfactants such as oleic acid can be chosen as the capping reagent. Due to the effect of organic surfactant, the obtained nanostructures have a controllable shape and smaller size. According to the theory stated above, we propose a basic understanding of the reaction process for the formation of the $LaPO_4:Ln^{3+}$ nanocrystals as shown schematically in Scheme 1. In a typical synthetic process, oleic acid, which has a long alkyl chain and can effectively adsorbed on the surfaces of the products, was chosen as the capping reagent to control the growth of the $LaPO_4$ particles. Ethanol has been adopted as the common solvent for oleic acid and water so that the complexation process of oleic acid and metal ions can occur under a relative homogeneous condition. NaOH was employed to convert the oleic acid to sodium oleate which will ensure an ion exchange process to form the metal oleate. As depicted, a solution which contained oleic acid, NaOH, and ethanol is first induced to form a sodium oleate solution. In this procedure, two phases have been formed, including the liquid phase consisting of the excess oleic acid and ethanol, and the solid phase contains sodium oleate. Then an aqueous solution containing M^{3+} (M = La, Eu) is added to form a third phase (the solution phase). Meanwhile, a phase transfer process occurs in which the M^{3+} shifts from the aqueous solution to the solid phase of *n*(RCOO)M. After the addition of PO_4^{3-}, the oleic acid capped M^{3+} reacted with PO_4^{3-} quickly to form an oleic acid capped MPO_4 amorphous precipitation. Then the system experiences a typical hydrothermal crystallization and ripening process assisted by the mixed surfactant at a designated temperature. After that, phase separation may occur due to the high density of the $LaPO_4:Ln^{3+}$ nanocrystals and their hydrophobic surfaces, and $LaPO_4:Ln^{3+}$ particles could be collected at the bottom of the vessel.

3.3. Photoluminescence (PL) and kinetic properties

The as-synthesized $LaPO_4:Eu^{3+}$, $LaPO_4:Ce^{3+}$, and $LaPO_4:Ce^{3+},Tb^{3+}$ nanocrystals show the respective red, blue, and green emissions under ultraviolet (254 nm) irradiation, as shown in Fig. 5. The fluorescent properties of $LaPO_4:Eu^{3+}$, $LaPO_4:Ce^{3+}$, and $LaPO_4:Ce^{3+},Tb^{3+}$ was further investigated by the PL excitation and emission spectra (Fig. 6). As shown, the excitation spectrum of $LaPO_4:Eu^{3+}$ (Fig. 6a, left), which is monitored by the 594 nm emission of Eu^{3+} ($^5D_0$–$^7F_1$), consists of a broad band with a maximum at 251 nm and a week peak at about 395 nm. The broad band at 251 nm is due to the charge transfer band (CTB) of the transition from the 2p orbital of oxygen to the 4f orbital of the europium [51]. And the weak line at 395 nm may arise from the direct excitation of the f–f shell transitions of the Eu^{3+} ions [34]. In the emission spectrum upon excitation at 251 nm (Fig. 6a, right), the $^5D_0$–^7F_J (J = 1, 2, 3) emission lines can be detected, which correspond to the peaks located at 594 ($^5D_0$–$^7F_1$), 615 ($^5D_0$–$^7F_2$), 650 nm ($^5D_0$–$^7F_3$), respectively [52–54]. Furthermore, no emission from the higher energy levels ($^5D_1$, $^5D_2$) of the Eu^{3+} ions can be detected due to the multiphoton relaxation derived from the vibration of phosphate groups, which can effectively bridge the gaps between the higher energy levels ($^5D_1$, $^5D_2$) and the lowest level ($^5D_0$). It should be noticed that the luminescent spectra of Eu^{3+} ion in our work show some difference from the paper [55], in which the maximum peak in the excitation spectrum for Eu^{3+} is only located at 393 nm. While our work also relates to the spectrum at less 300 nm. For the $LaPO_4:Ce^{3+}$ phosphors (Fig. 6b), the emission spectrum shows a broad band with a maximum at 365 nm, which may be assigned to the parity-allowed transitions of the lowest component of the 2D state to the spin-orbit components of the ground state. Monitored by the emission wavelength at 365 nm, the excitation spectrum consists of two peaks with maxima at 279 and 241 nm, which can correspond to the transitions from the ground state $^2F_{5/2}$ of Ce^{3+} to different crystal field components of the excited Ce^{3+} 5d levels [56]. The excitation spectrum of $LaPO_4:Ce^{3+},Tb^{3+}$ (Fig. 6c, left) recorded at the 542 nm

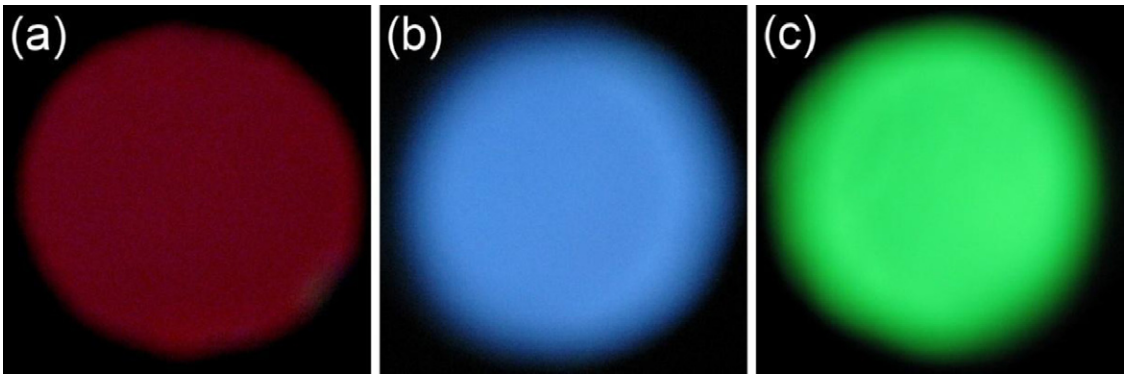

Fig. 5. Photographs of $LaPO_4:Eu^{3+}$ (a), $LaPO_4:Ce^{3+}$ (b), and $LaPO_4:Ce^{3+},Tb^{3+}$ (c) irradiated by a 254 nm UV lamp in dark.

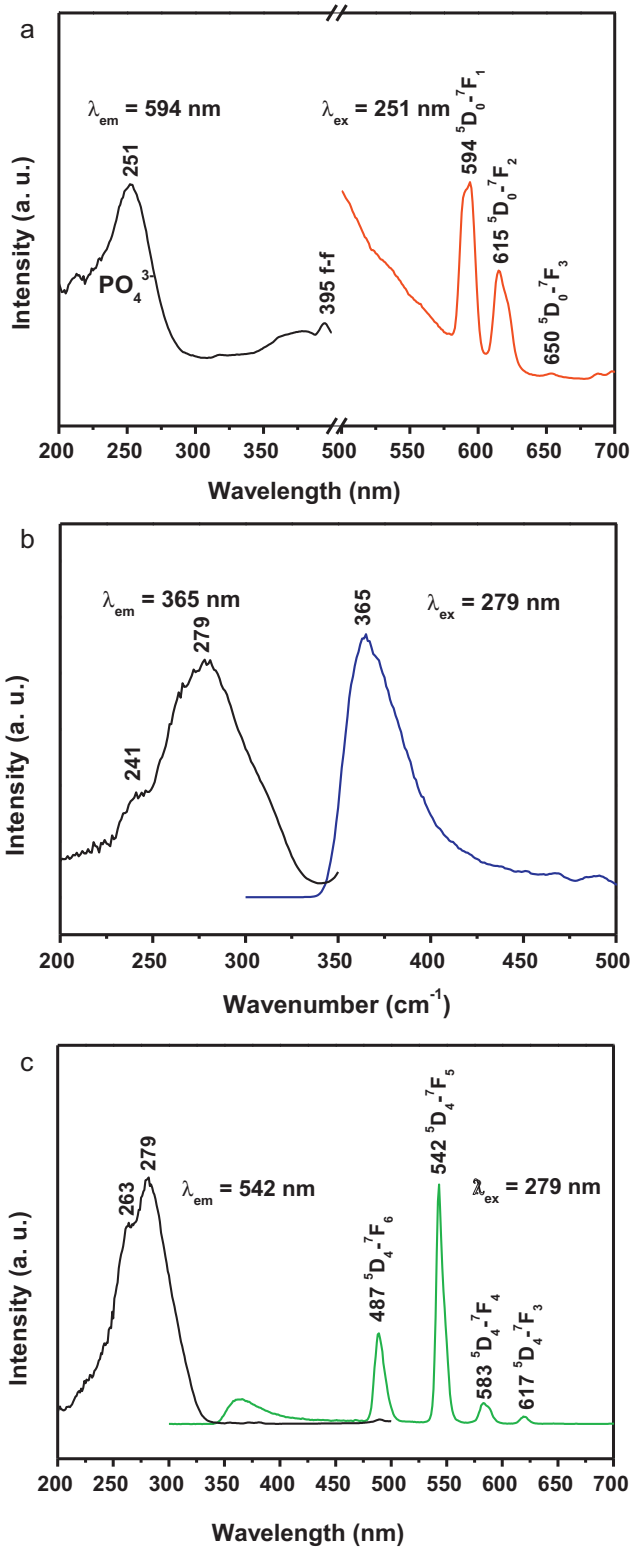

Fig. 6. Excitation (left) and emission (right) spectra of as-synthesized $LaPO_4:Eu^{3+}$ (a), $LaPO_4:Ce^{3+}$ (b), and $LaPO_4:Ce^{3+},Tb^{3+}$ (c).

emission ($^5D_4$–$^7F_5$) is exclusively composed of excitation bands of Ce^{3+}. The emission spectrum of $LaPO_4:Ce^{3+},Tb^{3+}$ excitation at 279 nm involves the weak emission of Ce^{3+} (300–360 nm) and the strong emission of Tb^{3+} maximum at 487 nm ($^5D_4$–$^7F_6$), 542 nm ($^5D_4$–$^7F_5$), 583 nm ($^5D_4$–$^7F_4$), 617 nm ($^5D_4$–$^7F_3$). This suggests an energy transfer from Ce^{3+} to Tb^{3+} in $LaPO_4:Ce^{3+},Tb^{3+}$, which is well consistent with the bulk $LaPO_4:Ce^{3+},Tb^{3+}$ [56].

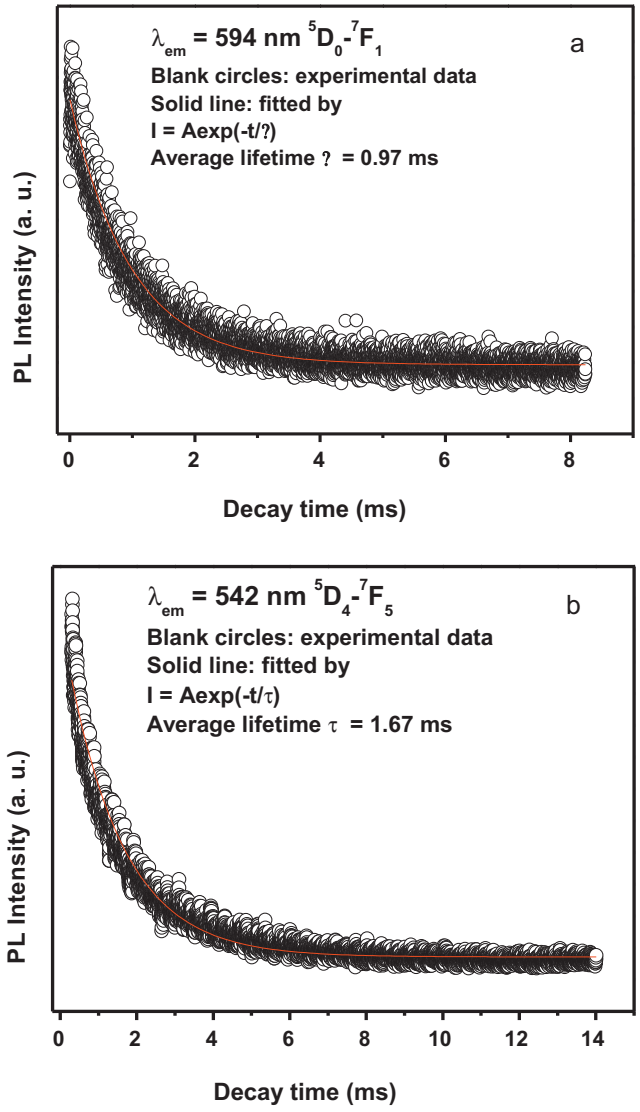

Fig. 7. Decay curves for the luminescence of Eu^{3+} in $LaPO_4:Eu^{3+}$ (a) and Tb^{3+} in $LaPO_4:Ce^{3+},Tb^{3+}$ (b).

By monitoring the emission of Eu^{3+} ion at 594 nm, the decay curve for $^5D_0$–$^7F_2$ emission can be detected, as shown in Fig. 7a. It can be seen that the curve can be well fitted into a single exponential function as $I(t) = I_0 \exp(-t/\tau)$ (where τ is the $1/e$ life time of the Eu^{3+} ion), yielding to lifetime value of 0.97 ms for Eu^{3+} in the $LaPO_4:Eu^{3+}$ nanocrystals. Decay curve for the luminescence of Tb^{3+} in $LaPO_4:Ce^{3+},Tb^{3+}$ is depicted in Fig. 7b, which is much similar to the single exponential luminescence decay of Eu^{3+} in the $LaPO_4:Eu^{3+}$ phosphors, and the luminescence lifetime of Tb^{3+} is calculated to be 1.67 ms.

4. Conclusions

In summary, $LaPO_4:Ln^{3+}$ (Ln = Eu, Ce, Tb) nanoparticles have been successfully synthesized through solvothermal method assisted by the capping agent (oleic acid) without further heat treatment. The obtained particles exhibit a relatively uniform morphology in a narrow size distribution with an average size of about 15 nm. The as-synthesized $LaPO_4:Eu^{3+}$ and $LaPO_4:Ce^{3+},Tb^{3+}$ samples show strong light emissions with red and green colors of Eu^{3+} and Tb^{3+} ions, respectively. The decay curves of all the samples can be well fitted into a single exponential function. These phos-

phors exhibit potential applications in the display fields due to their special properties.

Acknowledgments

This project is financially supported by the National Natural Science Foundation of China (NSFC 20871035), China Postdoctoral Special Science Foundation (200808281), and Harbin Sci-Tech Innovation Foundation (No. 2009RFQXG045).

References

[1] Y.F. Zhu, H.G. Pan, M.X. Gao, J.X. Ma, Y.Q. Lei, Q.D. Wang, Int. J. Hydrogen Energy 28 (2003) 311.
[2] H.G. Pan, F.M. Yang, C.P. Chen, N. Tang, X.F. Han, Q.D. Wang, J. Magn. Magn. Mater. 163 (1996) 221.
[3] A.A. Dakhel, J. Alloys Compd. 470 (2009) 195.
[4] Y.F. Liu, H.G. Pan, M.X. Gao, L. Rui, X.Z. Sun, Y.Q. Lei, J. Alloys Compd. 388 (2005) 109.
[5] F. Li, M. Wang, C. Mi, K. Yi, S. Xu, J. Alloys Compd. 486 (2009) 37.
[6] Y. Mayama, T. Masui, K. Koyabu, N. Imanaka, J. Alloys Compd. 451 (2008) 132.
[7] Y.F. Xu, D.K. Ma, M.L. Guan, X.A. Chen, Q.Q. Pan, S.M. Huang, J. Alloys Compd. 502 (2010) L38.
[8] J.X. Meng, F.J. Zhang, W.F. Peng, W.J. Wan, Q.L. Xiao, Q.Q. Chen, J. Alloys Compd. 508 (2010) 222.
[9] S. Romankov, Y. Hayasaka, N. Hayashi, E. Kasai, S. Komarov, J. Alloys Compd. 495 (2010) 625.
[10] H.G. Pan, S. Ma, J. Shen, J.J. Tan, J.L. Den, M.X. Gao, Int. J. Hydrogen Energy 14 (2007) 2949.
[11] C. Feldman, T. Jüste, C. Ronda, P. Schmidt, Adv. Funct. Mater. 13 (2003) 511.
[12] G. Blasse, Chem. Mater. 6 (1994) 1465.
[13] H.G. Pan, Q.W. Jin, M.X. Gao, Y.F. Liu, R. Li, Y.Q. Lei, Q.D. Wang, J. Alloys Compd. 376 (2004) 196.
[14] A.A. Dakhel, J. Alloys Compd. 488 (2009) 31.
[15] T. Jin, S. Tsutsumi, Y. Deguchi, K. Machida, G. Adachi, J. Alloys Compd. 252 (1997) 59.
[16] Y. Hikichi, T. Ota, K. Daimon, T. Hattor, M. Mizuno, J. Am. Ceram. Soc. 81 (1998) 2216.
[17] B. Yan, J. Gu, J. Alloys Compd. 479 (2009) 536.
[18] C. Guo, Y. Xu, X. Ding, M. Li, J. Yu, Z. Ren, J. Alloys Compd. 509 (2011) L38.
[19] L. Xu, G. Guo, D. Uy, A. O'Neil, W.H. Weber, M.J. Rokosz, R.W. McCabe, Appl. Catal. B 50 (2004) 113.
[20] K. Rajesh, P. Mukundan, P.K. Pillai, V.R. Nair, K.G.K. Warrier, Chem. Mater. 16 (2004) 2700.
[21] C.C. Tang, Y. Bando, D. Golberg, R. Ma, Angew. Chem. Int. Ed. 44 (2005) 5766.
[22] H.C. Lu, G.S. Yi, S.Y. Zhao, D.P. Chen, L.H. Guo, J.J. Cheng, J. Mater. Chem. 14 (2004) 1336.
[23] G. Blasse, B.C. Grabmaier, M. Ostertag, J. Alloys Compd. 200 (1993) 17.
[24] X. Jing, T.G. Ireland, C. Gibbons, D.J. Barber, J. Silver, A. Vecht, G. Fern, P. Trogwa, D. Morton, J. Electrochem. Soc. 146 (1999) 4546.
[25] G.Y. Adachi, N. Imanaka, Chem. Rev. 98 (1998) 1479.
[26] M. Haase, K. Riwotzki, H. Meyssamy, A. Kornowski, J. Alloys Compd. 303 (2000) 191.
[27] K. Riwotzki, H. Meyssamy, H. Schnablegger, A. Kornowski, M. Haase, Angew. Chem. Int. Ed. 40 (2001) 573.
[28] F.H. Firsching, S.N. Brune, J. Chem. Eng. Data 36 (1991) 93.
[29] A. Rouanel, J.J. Serra, K. Allaf, V.P. Orlovskii, Inorg. Mater. 17 (1981) 76.
[30] Y. Guo, P. Woznicki, A. Barkatt, E.E. Saad, I.G. Talmy, J. Mater. Res. 11 (1996) 639.
[31] S. Ding, D. Zhang, P. Wang, J. Wang, Mater. Chem. Phys. 68 (2001) 98.
[32] Y.C. Kang, E.J. Kim, D.Y. Lee, H.D. Park, J. Alloys Compd. 347 (2002) 266.
[33] L. Ma, L.M. Xu, W.X. Chen, Z.D. Xu, Mater. Lett. 63 (2009) 1635.
[34] M. Yu, J. Lin, J. Fu, H.J. Zhang, Y.C. Han, J. Mater. Chem. 13 (2003) 1413.
[35] W. Di, X. Wang, B. Chen, H. Lai, X. Zhao, Opt. Mater. 27 (2005) 1386.
[36] Y.C. Shang, P.P. Yang, W.X. Wang, Y.L. Wang, S.L. Gai, J. Lin, J. Alloys Compd. 509 (2011) 837.
[37] X.Y. Wu, H.P. You, H.T. Cui, X.Q. Zeng, G.Y. Hong, C.H. Kim, C.H. Pyun, B.Y. Yu, C.H. Park, Mater. Res. Bull. 37 (2002) 1531.
[38] G.C. Han, Y.H. Wang, C.F. Wu, J.C. Zhang, Mater. Res. Bull. 44 (2009) 2255.
[39] H.L. Zhu, E. Zhu, H. Yang, L. Wang, D.L. Jin, K.H. Yao, J. Am. Ceram. Soc. 91 (2008) 1682.
[40] M. Yu, H. Wang, C.K. Lin, G.Z. Li, J. Lin, Nanotechnology 17 (2006) 3245.
[41] R.C.L. Mooney, Acta Crystallogr. 3 (1950) 337.
[42] M.H. Cao, C.W. Hu, Q.Y. Wu, C.X. Guo, Y.J. Qi, E.B. Wang, Nanotechnology 16 (2005) 282.
[43] C.R. Patra, G. Alexandra, S. Patra, D.S. Jacob, A. Gedanken, A. Landau, Y. Gofer, New J. Chem. 29 (2005) 733.
[44] J.C. Yu, L.Z. Zhang, Z. Zheng, J.C. Zhao, Chem. Mater. 15 (2003) 2280.
[45] V. Koleva, E. Zhecheva, R. Stoyanova, J. Alloys Compd. 476 (2009) 950.
[46] L. Li, W. Jiang, H.H. Pan, X.R. Xu, Y.X. Tang, J.Z. Ming, Z.D. Xu, R.K. Tang, Phys. Chem. C 111 (2007) 4111.
[47] X. Wang, J. Zhuang, Q. Peng, Y.D. Li, Nature 437 (2005) 121.
[48] X. Zhang, Z. Quan, J. Yang, P. Yang, H. Lian, J. Lin, J. Colloid Interface Sci. 329 (2009) 103.
[49] F. Zhang, J. Li, J. Shan, L. Xu, D.Y. Zhao, Chem. Eur. J. 15 (2009) 11010.
[50] W.B. Bu, Z.X. Chen, F. Chen, J.L. Shi, J. Phys. Chem. C 113 (2009) 12176.
[51] P.P. Yang, Z.W. Quan, C.X. Li, Z.Y. Hou, W.X. Wang, J. Lin, J. Solid State Chem. 182 (2009) 1045.
[52] D.L. Shi, J. Lian, W. Wang, G.K. Liu, P. He, Z.Y. Dong, L.M. Wang, R.C. Ewing, Adv. Mater. 18 (2006) 189.
[53] K. Riwotzki, H. Meyssamy, A. Kornowski, M. Haase, J. Phys. Chem. B 104 (2000) 2824.
[54] G. Buhler, C. Feldmann, Appl. Phys. A 87 (2007) 631.
[55] Z.L. Xiu, S.W. Liu, M.K. Lu, H.P. Zhang, G.L. Zhou, Mater. Res. Bull. 41 (2006) 642.
[56] V. Buissette, M. Moreau, T. Gacoin, J.P. Boilot, Adv. Funct. Mater. 6 (2006) 351.